Accepted Manuscript

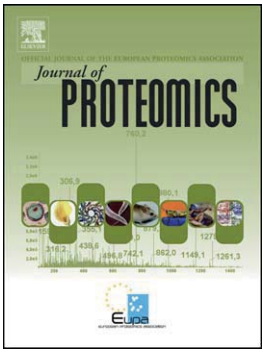

RNAi-mediated downregulation of poplar plasma membrane intrinsic proteins (PIPs) changes plasma membrane proteome composition and affects leaf physiology

Zhen Bi, Juliane Merl-Pham, Norbert Uehlein, Ina Zimmer, Stefanie Mühlhans, Michaela Aichler, Axel Karl Walch, Ralf Kaldenhoff, Klaus Palme, Jörg-Peter Schnitzler, Katja Block

PII: S1874-3919(15)30082-8
DOI: doi: 10.1016/j.jprot.2015.07.029
Reference: JPROT 2234

To appear in: *Journal of Proteomics*

Received date: 29 May 2015
Revised date: 16 July 2015
Accepted date: 23 July 2015

Please cite this article as: Bi Zhen, Merl-Pham Juliane, Uehlein Norbert, Zimmer Ina, Mühlhans Stefanie, Aichler Michaela, Walch Axel Karl, Kaldenhoff Ralf, Palme Klaus, Schnitzler Jörg-Peter, Block Katja, RNAi-mediated downregulation of poplar plasma membrane intrinsic proteins (PIPs) changes plasma membrane proteome composition and affects leaf physiology, *Journal of Proteomics* (2015), doi: 10.1016/j.jprot.2015.07.029

RNAi-mediated downregulation of poplar plasma membrane intrinsic proteins (PIPs) changes plasma membrane proteome composition and affects leaf physiology

Zhen Bi[1], Juliane Merl-Pham[2], Norbert Uehlein[3], Ina Zimmer[1], Stefanie Mühlhans[1], Michaela Aichler[4], Axel Karl Walch[4], Ralf Kaldenhoff[3], Klaus Palme[5], Jörg-Peter Schnitzler[1] and Katja Block[1*]

[1]Research Unit Environmental Simulation, Institute of Biochemical Plant Pathology, [2]Research Unit Protein Science-Core Facility Proteomics, [4]Research Unit Analytical Pathology, Helmholtz Zentrum München, Ingolstädter Landstr.1 85764 Neuherberg, Germany,

[3]Institute of Applied Plant Science, University of Technology Darmstadt, Schnittspahndtr.10, 64287 Darmstadt, Germany,

[5]BIOSS Centre for Biological Signalling Studies; ZBSA Centre for Biosystems Studies; Faculty of Biology, Schänzlestr. 1, University of Freiburg, 79104 Freiburg, Germany

* For correspondence (e-mail katja.block@helmholtz-muenchen.de)

Abstract

Plasma membrane intrinsic proteins (PIPs) are one subfamily of aquaporins that mediate the transmembrane transport of water. To reveal their function in poplar, we generated transgenic poplar plants in which the translation of *PIP* genes was downregulated by RNA interference investigated these plants with a comprehensive leaf plasma membrane proteome and physiome analysis. First, inhibition of PIP synthesis strongly altered the leaf plasma membrane protein composition. Strikingly, several signaling components and transporters involved in the regulation of stomatal movement were differentially regulated in transgenic poplars. Furthermore, hormonal crosstalk related to abscisic acid, auxin and brassinosteroids was altered, in addition to cell wall biosynthesis/cutinization, the organization of cellular structures and membrane trafficking. A physiological analysis confirmed the proteomic results. The leaves had wider opened stomata and higher net CO_2 assimilation and transpiration rates as well as greater mesophyll conductance for CO_2 (g_m) and leaf hydraulic conductance (K_{leaf}). Based on these results, we conclude that PIP proteins not only play essential roles in whole leaf water and CO_2 flux but have important roles in the regulation of stomatal movement.

Key words: aquaporin; PIP, plasma membrane intrinsic protein; *Populus* × *canescens*; plasma membrane proteomics; photosynthesis; stomatal movement

1. Introduction

Plasma membrane intrinsic proteins (PIPs) are one subfamily of aquaporins (AQPs) that mediate the transmembrane transport of water thereby controlling water permeability and plant hydraulics at the cell, tissue, organ and whole plant level (for review see [1–5]). Besides the overall role in enabling the transmembrane water transport, they can have specialized functions, for instance in the stomatal complexes [6], in facilitating the lateral root emergence [7] or in controlling the radial water unloading from xylem into the bundle-sheath cells [8]. Studies with woody species revealed specific functions of PIPs for instance in root [9,10] and leaf [11] hydraulic conductance, in the recovery from embolism [12,13] and in the communication and regulation of shoot-root water homeostasis [14,15].

In addition to water, some PIPs transport other small molecules such as glycerol and urea (reviewed in [16]). An increasing amount of experimental evidence indicates that specific PIPs transport CO_2 and are involved in the control of mesophyll CO_2 conductance (g_m) in leaves. In 2003, Uehlein *et al.* [17] noted that the overexpression of NtAQP1 in tobacco increased CO_2 membrane permeability; in contrast, the antisense plants displayed reduced membrane permeability for CO_2. Increases in the internal CO_2 conductance and net CO_2 assimilation have been observed also in barley (*Hordeum vulgare*) overexpressing HvPIP2;1 [18]. In Arabidopsis leaves, AtPIP1;2 was found to limit CO_2 diffusion and photosynthesis [19]. Recently, it was also demonstrated in poplar, a woody species, that the reduction of PIP1s impairs leaf membrane permeability to CO_2 [20]. And also in olive trees, PIPs regulate stomatal (g_s) and mesophyll (g_m) conductance to CO_2 [21].

The conductance of water and CO_2 are important constraints of the overall process of carbon fixation and must be understood in detail to optimize the photosynthetic capacity and water use efficiency (WUE). Poplars are perennial, fast growing trees and generally possess a high photosynthetic capacity. Therefore, they have been proposed to be an important renewable bioenergy resource and are being planted increasingly in high density plantations for biomass production [22]. In nature, most poplar species prefer moist habitats and consume large amounts of water [23]; however, plantations are typically established on marginal land with limited water and nutrients [24]. Therefore, enhancing the water use

efficiency (WUE) in parallel with the photosynthetic capacity and biomass production are important traits for optimization in poplar.

The PIP subfamily of aquaporins clusters in the phylogenic subgroups PIP1 and PIP2, which differ in the lengths of their N- and C-termini. There are 13 *PIP* genes in Arabidopsis and maize [3,25], and there are 15 *PIP* genes in *Populus trichocarpa* [26].

The main objective of this study was to generate transgenic grey poplar (*P.* × *canescens*) plants with reduced PIP1s and PIP2s to investigate the functionality and importance of PIPs for leaf water and CO_2 transport on the cellular and whole plant level in this fast-growing tree species.

2. Material and methods

2.1. Construction of binary vectors, plant transformation and cultivation

To explore the function of PIPs in *Populus* × *canescens* (syn. *P. tremula* × *P. alba,* number 7171-B4, Institut de la Recherche Agronomique, Nancy, France), transgenic lines with reduced *PIP* gene expression were generated using RNA interference (RNAi). The highly conserved *PIP*-specific H5/NPA Loop E region [27] was selected for two different RNAi constructs: the first sequence was used to target PIPs of subtype 1 (180 bp = *PcPIP*-I-RNAi), and the second was used to target PIPs of subtype 2 (164 bp = *PcPIP*-II-RNAi).

The potential targets of the two RNAi constructs were estimated with a multiple sequence alignment (CLUSTAL 2.1, http://www.genome.jp/tools-bin/clustalw, [28] of the *PcPIP*-I-RNAi and the *PcPIP*-II-RNAi sequences with the coding sequences of the 15 *P.* x *canescens* PIPs (*PcPIPs*) was performed. The 21-oligomers are considered to be the dominant class of RNA silencing-inducing siRNAs in plants [29,30], including poplar [31,32]. Therefore, the number of 21-oligomers with 100% identity was counted (Figure S1 and Table S1): the *PcPIP*-I-RNAi construct targets three *PIP1* genes (*PcPIP1;1*, *PcPIP1;2* and *PcPIP1;4*), the *PcPIP*-II-RNAi construct seven *PIP2* genes (*PcPIP2;1*, *PcPIP2;3 to PcPIP2;8*). In addition, an on/off-target analysis was performed using the two RNAi sequences for a BLAST of the *Populus trichocarpa* genome (Supplemental Table S2). For this purpose, gene annotation for the poplar genome was downloaded from Ensembl Plants [33] in its version 2.0. For all genes, cDNA sequences including flanking 250 base pairs upstream and downstream of the transcription start site were extracted from

BioMart [34]. *PcPIP*-RNAi sequences were searched against this sequence database using BLASTN [35] with standard parameters and no e-value cutoff to not miss short alignments. The on/off-target analysis revealed no additional targets of the 2 RNAi sequences besides *PIP* genes.

The RNAi sequence synthesis, cloning into vector p9U10 (a special vector containing two inverted 35S promoter sequences to constitutively produce the sense and antisense strand) and transformation into *Agrobacterium tumefaciens* GV310 (PMP90RK) was performed by the DNA Cloning Service e.K. Germany, (http://www.dna-cloning.com). The final transformation of *P.* x *canescens* with the 35S::*PcPIP*-I-RNAi-construct, the 35S::*PcPIP*-II-RNAi-construct and p9U10 empty vector as a control was conducted as described by Meilan and Ma [36].

Transgenic RNAi poplar plants were amplified by micropropagation as described by Behnke *et al.,* [37] and cultivated in 1-L glass containers at 22±1°C during the day and 20±1°C at night with a photoperiod of L16 h:D8 h and a light intensity of 120 µmol m^{-2} sec^{-1} PPFD. After 3 months, the rooted shoots were transferred first to 0.2-L pots containing soil substrate [50% v/v Fruhstorfer Einheitserde Typ N 50% v/v silica sand (particle size 2–3 mm)] for acclimatization in a propagator, and then to 2.2-L pots with soil substrate [50% v/v Fruhstorfer Einheitserde Typ T, 25% (v/v) silica sand and 25% (v/v) perlite] containing 10 g fertilizer [Triabon (Compo) and Osmocote (Scotts International BV), 1:1 v/v per liter of soil] for cultivation in the greenhouse.

2.2. Cloning of the *P.* x *canescens* PIP gene family

Primers for cloning the *P.* x *canescens PIP* gene family were designed based on the *P. trichocarpa PIP* gene accessions identified by [26], and the most recent sequences (genome version 3.0, Phytozome v 9.1) (Table S3). PCR was performed using 5 U High Fidelity Taq DNA polymerase (Life Technologies GmbH, Darmstadt Germany) and PCR products were cloned into pCRTM 4-TOPO (Life Technologies GmbH, Darmstadt Germany). The obtained *P.* x *canescens* sequences were confirmed by sequencing (Genbank accessions: KP940359, KP940360, KP940361, KP940362, KP940363, KP940364, KP940365, KP940366, KP940367, KP940368, KP940369, KP940370, KP940371, KP940372 and KP966101).

2.3. Molecular screening by semi-quantitative RT-PCR and ELISA (Enzyme-Linked ImmunoSorbent Assay)

For sqRT-PCR and ELISA analysis, leaf no. 9 of 3 plants per genotype (13 *PcPIP*-I-RNAi lines, 7 *PcPIP*-II-RNAi lines and empty vector control) was harvested at mid-day (12:00-13:00), immediately frozen in liquid nitrogen and stored at -80°C prior to use. Total RNA was extracted from 50 mg frozen leaf material using the Aurum Total RNA Mini kit (Bio-Rad, Germany) and cDNAs were synthesized with an Omniscript RT kit (Qiagen, Germany) using 1 µg RNA. The sqRT-PCR of 4 highly expressed leaf-specific *PIP* genes (*PIP1;1, PIP1;2, PIP2;5* and *PIP2;6*; for primers see Table S4) was performed using 2 µL of synthesized cDNA as a template and the Taq DNA polymerase (Life Technologies GmbH, Darmstadt Germany). After the PCR products were subjected to agarose gel electrophoresis and stained with ethidium bromide, quantification was performed using ImageJ (http://imagej.nih.gov/ij/docs/index.html ImageJ user guide).

For production of PIP subtype 1 or 2-specific rabbit monoclonal antibodies, the *PcPIP* sequences were translated into protein sequences using DNASTAR software. With the HUSZAR program, the secondary structure of the PIPs was analyzed to design and synthesize 2 subtype-specific peptides for each group: peptide 1 and 2 for PIP1s (MEGKEEDVRLGANKFNERQP, AQSQDDKDYKEPPP) and peptide 3 and 4 for PIP2s (MSKEVIEEGHTHGKDYVDPP, MGKDIEVGSEFIAKDYHDPP) which were further used for rabbit immunization and antibody production. For ELISA, 150 mg leaf powder and 75 mg polyclar® AT (Sigma-Aldrich Chemie GmbH, Taufkirchen bei München, Germany) were mixed with 1.5 mL homogenization buffer (0.33 M Sucrose, 50 mM MOPS-KOH pH 7.5, 5 mM EDTA, 0.2% (w/v) casein, 5 mM DTT, 5 mM ascorbic acid, 0.5 mM PMSF and protease inhibitor) to first extract the microsomal fractions. After 15-min incubation on ice, the mixture was filtered and centrifuged (15 min, 10,000*g*). The supernatant was centrifuged again for 75 min at 23,000 g; then the pellet was re-suspended in 200 µl 100 mM carbonate/bicarbonate buffer (pH 9.5). One hundred microliters diluted protein (1 µg ml^{-1}) was incubated in 96-well plates at 4°C overnight for protein binding, followed by blocking with 300 µL 1% (w/v) caseinate in PBS-T (37°C, 1 h), antibody incubation with either the PIP1 or PIP2 antibody mix (37°C, 1 h), and 5 washes with PBS-T. After incubation with the anti-rabbit horseradish peroxidase (HRP) antibody (Peptide Specialty Laboratories GmbH, Germany) at 37°C for 1 h, two washes with PBS-T and three washes with PBS, 100 µL 3,3',5,5'-Tetramethylbenzidine (TMB, Sigma-Aldrich) was added to each well

and incubated for 20 min at 37°C. Finally, the reaction was stopped with 100 µl 1 M H_2SO_4. The absorbance was measured at 450 nm using an Ultrospec 3100 pro (GE, Pittsburgh, Pennsylvania, USA).

2.4. Proteomics of plasma membrane proteins

Sample preparation

Plasma membranes from leaves were isolated according to the procedure of Kjellbom and Larsson [38]. Fresh leaf material of 4 plants per genotype (7.5 g, leaf no.6-8 and 10-12 harvested at 9:00) with 0.6 g polyclar® AT was homogenized 5 times for 10 s in 50 mL homogenization buffer using a blender. The homogenate was filtered through two layers of nylon cloth and centrifuged at 10,000 *g* for 15 min. The membranes in the supernatant were precipitated at 30,000 *g* for 1 h, and the pellet was re-suspended in a total volume of 5 mL in 0.33 M sucrose, 5 mM potassium phosphate (pH 7.8), 0.1 mM EDTA-KOH (pH 7.8), 1 mM DTT and protein inhibitor. Plasma membranes were purified from the crude membrane fraction using the two-phase partitioning system [39,40]. The microsomal suspension (4.5 ml) was added to 13.5 g of the phase mixture (6.1% (w/w) Dextran T 500, 6.1% (w/w) polyethylene glycol 3350, 0.33 M sucrose, 0.15 mM potassium phosphate buffer (pH 7.8), 0.9 mM KCl). The phase system was mixed by several inversions and centrifuged using a swing-out rotor for 5 min at 1500 *g*. The upper phase was re-extracted 3 times. The plasma membrane–enriched final upper phase was diluted in 70 mL buffer and centrifuged at 100,000 *g* for 1 h. The pellet was re-suspended in 8 M urea in 0.1 M Tris/HCl (pH 8.5) for tryptic digestion using a modified FASP procedure [41]. Ten micrograms were reduced using 100 mM dithiothreitol and alkylated with 10 µL of 300 mM iodoacteamide. The samples were transferred to a 30-kD centrifuge filter (Pall Corporation, Washington, New York, USA), repeatedly washed with 8 M urea in 0.1 M Tris/HCl, pH 8.5, followed by washes with 50 mM ammonium bicarbonate, then cleaved with 1 µg Lys-C (Wako Chemicals GmbH, Neuss, Germany) for 2 h at room temperature and digested with trypsin (Promega) at 37 ºC overnight. The digested peptides were collected by centrifugation and acidified with trifluoracetic acid prior to the LC-MS/MS analysis.

LC-MS/MS-based Mass Spectrometry, Label-free Peptide Quantification and Protein Identification

The separation and analysis of proteins was performed as previously described [42,43] using an Ultimate 3000 nano-HPLC system (Dionex, Thermo Scientific, Bremen, Germany) coupled to an LTQ OrbitrapXL (Thermo Scientific, Bremen, Germany). Each sample (0.5 µg) was automatically injected and loaded onto the trap column at a flow rate of 30 µL min^{-1} in 97% buffer A (2% ACN / 3% DMSO / 0.1% formic acid (FA)) and 3% buffer B (73% ACN / 3% DMSO / 0.1% FA) [44]. After 5 min, the peptides were eluted and separated at a flow rate of 300 nL min^{-1} on the analytical column (75 µm i.d. × 25 cm, Acclaim PepMap100 C18, 3 µm, 100 Å, Dionex, Idstein, Germany) for 140 min using an acetonitrile gradient from 3% to 35% of buffer B, followed by a 5 min gradient from 35% to 95% buffer B and final equilibration for 20 min with 3% buffer B. From the MS prescan, the 10 most abundant peptide ions were fragmented by collision-induced dissociation in the linear ion trap if they displayed an intensity of at least 200 counts and had a charge of at least +2, with a dynamic exclusion of 60 sec. During fragmentation, a high-resolution (full width of 60,000 at half-maximum) MS spectrum was acquired in the Orbitrap with a mass range from 300 to 1,500 Da.

The acquired spectra were loaded into Progenesis LC−MS software (version 2.5, Nonlinear Dynamics) and analyzed applying a label-free peptide quantification, which is based on intensity and abundance of the corresponding peak area [42,43]. Features with only one charge or more than 8 charges were excluded from the analysis. The raw abundances of the remaining features were normalized to allow correction for factors resulting from experimental variation. All of the MS/MS spectra were exported as a Mascot generic file (mgf) and used for the peptide identification with MASCOT (version 2.3.02) in the *P. trichocarpa* protein database (version 3, 30195906 residues, 73013 sequences). The search parameters included a peptide mass of 10 ppm and tolerance of 0.6 Da MS/MS, one missed cleavage, cysteine carbamidomethylation as the fixed modification, and methionine oxidation and asparagine or glutamine deamidation as variable modifications. Using a MASCOT percolator score cutoff of 15 and a significance threshold of $P < 0.05$, the MASCOT-integrated decoy database search calculated a false discovery rate (FDR) of < 1%. The peptide assignments were reimported into Progenesis LC−MS software. Finally, only proteins represented by a minimum of two peptides were considered and their abundances were calculated after summing the abundances of all of the peptides allocated to each protein. For the

identification of PIPs, a small database comprising the 15 *P.* x *canescens* sequences was used. The mass spectrometry proteomics data have been deposited to the ProteomeXchange Consortium [45] via the PRIDE partner repository with the dataset identifier PXD002544.

Multivariate Statistics, Gene Ontology and Functional Annotation

To ensure that only integral proteins associated with the plasma membrane were considered for the multivariate data analysis and interpretation, lists of identified proteins were filtered for the Gene Ontology (GO) annotation "Plasma membrane" of the corresponding *A. thaliana* ortholog (http://www.arabidopsis.org/tools/bulk/go/index.jsp), which was obtained via the POPGENIE (http://www.popgenie.org) database.

A multivariate data analysis was conducted using principal component analysis (PCA) and the orthogonal partial least square regression (OPLS-DA) approach using the software package 'SIMCA-P' (v. 13.0.0.0, Umetrics, Umeå, Sweden). PCA was used to initially identify a potential separation among the WT, EV and *PcPIP*-RNAi lines. OPLS was used to identify discriminant proteins that significantly distinguished WT/EV (Y variable = 0) from the *PcPIP*-RNAi lines (Y variable = 1). Proteins with a Variable of Importance for the Projection value (VIP value) greater than 1 were defined as discriminant proteins.

2.5. Photosynthetic gas exchange analysis

Gas exchange measurements were performed with the portable gas exchange system GFS-3000 (Walz, Effeltrich, Germany) using leaf no. 9. The initial settings of the cuvette were a flow rate of 750 µmol s^{-1}, 16500 ppm H_2O, 380 ppm CO_2, a light intensity of 1500 µmol $m^{-2}s^{-1}$ PPFD and a leaf temperature of 25 ˚C. For the A/Ci curves, after a 30-min stabilization phase to reach the steady state, the CO_2 concentration was changed stepwise: 200 ppm, 100 ppm, 50 ppm, 20 ppm, 380 ppm, 650 ppm, 1000 ppm, 1500 ppm, and 2000 ppm. The mesophyll conductance for CO_2 (g_m), maximum carboxylation rate allowed by ribulose 1·5-bisphosphate carboxylase/oxygenase (Rubisco) ($V_{c\ max}$), rate of photosynthetic electron transport (based on the NADPH requirements) (J), triose phosphate use (TPU) and day respiration (R_d) were calculated using a curve fitting method [46,47] by applying the online tool described by Sharkey *et al.* [48]. For the VPD (vapor pressure deficit) dependency, after reaching steady state, the relative humidity was decreased stepwise: 75%, 50%, 25%, and 0%.

2.6. Leaf hydraulic conductance analysis

The leaf hydraulic conductance was measured using the high-pressure flow meter (HPFM, [49]) run with degassed distilled water. For the measurement, leaf no.10 was cut, petiole was recut immediately under water to maintain the petiole length at 2.5 cm and then connected with the HPFM. The leaf was kept under water to maintain a temperature of 30 ˚C and to prevent transpiration. The leaf hydraulic conductance was calculated as the slope of the water flow versus the transient pressure using HPFM software (DYNAMAX, Houston, TX, USA). The leaf hydraulic conductance was normalized to the leaf dry weight.

2.7. Analysis of the stomata

Two leaf discs from each leaf no. 9 were sampled at 1 p.m. from greenhouse grown plants (temperature 25 ˚C, relative humidity 55%) and immediately fixed in PFA-glutaraldehyde fixation buffer (2.5% paraformaldehyde, 2.5% glutaraldehyde in 0.1 M phosphate buffer) [50]. The stomata were observed under a fluorescence microscope (Carl Zeiss AxioVision Release 4.8, Jena, Germany) using the DAPI filter with maximum excitation and emission wavelengths of 385 nm and 475 nm, respectively. Finally, the pore length, width and area of the stomata were measured using Carl Zeiss AxioVision Release 4.8 analysis software.

2.8. Statistical analysis

Statistically significant differences between transgenic plants and WT plants were analyzed using one-way analysis of variance (ANOVA, Holm-Sidak, $P < 0.05$) with Sigmaplot V 12.0 (Systat Software Inc., San Jose, CA, USA).

3. Results

3.1. Comprehensive downregulation of PIPs by RNAi

To explore the function of PIPs in Grey Poplar (*P.* × *canescens*), we produced poplar lines in which the *PIP* gene expression was reduced using RNA interference (RNAi). To target the two main groups of PIPs, we constructed specific RNAi cassettes for *PIP1* and *PIP2*.

For the initial molecular screening, the transcript abundance of 4 highly expressed leaf-specific *PIP* genes (*PIP1;1*, *PIP1;2*, *PIP2;5* and *PIP2;6*) by semi-quantitative RT-PCR and protein quantity by ELISA was analyzed in leaf no. 9 of greenhouse cultivated plants. Eight out of the 13 *PcPIP*-I-RNAi lines and 5 out of the 7 *PcPIP*-II-RNAi lines showed a reduction of *PIP* transcript levels compared with the empty vector control (EV) (Supplemental Figure S2A). Moreover, 7 out of 13 the *PcPIP*-I-RNAi lines and all of the selected *PcPIP*-II-RNAi lines showed a reduction in PIP protein abundance (Supplemental Figure S2B). In general, independent from the intended RNAi target (*PIP1.x* or *PIP2.x* transcripts), a comprehensive reduction of both PIP subtypes was observed at the transcript and protein level.

3.2. Reduction of PIP abundance modifies the plasma membrane proteome

For the isoform-specific quantification of PIP proteins and to characterize other plasma membrane transport processes, we analyzed 2 pre-selected lines and WT/EV using a proteomic approach. The analyses were undertaken with wild type and empty vector control plants, as well as two pre-selected *PcPIP*-RNAi lines PIPI-9 and PIPII-13, which showed reduced PIP transcript and protein levels based on the molecular screening and, additionally, a visual leaf phenotype when grown under normal greenhouse conditions (as described later). To ensure the plasma membrane-specific interpretation of the data, only proteins with a Gene Ontology (GO) annotation “Plasma membrane” / ”Anchored to Plasma membrane” for the corresponding *A. thaliana* ortholog were included in the analysis. Finally, we identified 11 out of the 15 PIP isoforms and additional 510 plasma membrane proteins in the poplar leaf extracts (Table S5). Analysis of the abundance of the individual PIP isoforms revealed an almost identical pattern of downregulation of certain PIPs in the two *PcPIP*-RNAi transgenic lines PIPI-9 and PIPII-13 (Figure 1).

To identify other plasma membrane proteins that were differentially regulated as consequences of the downregulation of the PIP isoforms, a multivariate data analysis was applied using the data set from the PIPI-9 and PIPII-13, EV lines and WT. The principal component analysis (PCA) clearly separated WT/EV from PIPI-9 and PIPII-13 (Supplemental Figure S3). To identify the most responsible proteins for the separation into these two classes, we performed an OPLS-DA and calculated the Variable of Importance for the Projection value (VIP value) for each plasma membrane protein (Figure 2, Table S6). The statistical model provided a significant separation of the WT/EV from the *PcPIP*-RNAi lines (CV-ANOVA p = 0.0012) and explained 57.8% of the variation in component 1 (X). Component 2 (Y) explained 99.7% of the variation with a prediction accuracy of 95.15%. Among 510 of the subjected proteins, 167 had a VIP value > 1 and were therefore identified as discriminate proteins (Figure 2B). Eighty-five of these proteins were more abundant in PIPI-9 and PIPII-13, whereas 82 proteins were less abundant (Table S6). However, the Log_2 ratios of the protein abundance ranged from +1.9 to -1.6, reflecting moderate differences in the plasma membrane protein composition between the WT/EV and *PcPIP*-RNAi plants.

The GO SLIM categorization of these 167 discriminant proteins revealed prominent roles and functions of these proteins in biological processes related to various stress responses (‘response to stress/abiotic and biotic stimulus’, 20%), to the processes of ‘cell organization and biogenesis’/’development’ (11%) and to the ‘transport’ of substances (9%). Additionally, some proteins could be assigned to ‘protein metabolism’, ’signal transduction’, ‘transcription’, ‘DNA or RNA metabolism’, or ‘electron transport or energy pathways’ (Figure 3A).

Because the ‘response to stress and abiotic/biotic stimulus’ comprised proteins with versatile activities (e.g., ABC transporters, calcium-dependent protein kinases, glycosyl hydrolase), we examined the TAIR annotation and available literature information for each protein in detail. As a result, the proteins could be attributed to a more specific role in metabolism or physiology (e.g., “regulation of stomatal aperture and movement”, “cell wall biosynthesis”, “photosynthesis”) (Figure 3B and Supplemental Table S6).

Remarkably, various proteins related to guard cell development and the control of stomatal movement exhibited a differential abundance in *PcPIP*-RNAi plants. The ortholog of *A. thaliana* AtCDC2, a cyclin-dependent kinase involved in guard cell development, was downregulated in *PcPIP*-RNAi leaves. The abundance of several guard cell signaling components (orthologs of AtCBL1, AtCPK3, AtCPK6, AtHsp70-15, AtPCAP1, AtPLDDELTA and AtTCTP) was altered, implying changes in guard cell regulation. In addition to the proteins involved in signaling, several proton pumps (e.g., AtAHA5, AtAVP1 and AtVHA), ion transporters (e.g., AtKAB1, AtNRT1.3, AtVDAC1 and AtACA2) and sugar transporters (AtSTP13 and AtSUT4) were downregulated, excluding AtAHA5, which was upregulated. The transport of all of these substances (H^+, K^+, NO_3^-, sugars), which contribute to osmosis driven stomatal movement [51], appeared to be affected in response to PIP downregulation.

Consistent with the role of PIPs in controlling transmembrane water transport and thereby the balance of water in the whole leaf is the observation that 23 differentially regulated proteins were involved in abscisic acid (ABA) signaling and related to dehydration/osmotic stress. Interestingly, AtPERK4, which plays a positive role in ABA signaling, was downregulated, whereas two negative regulators of ABA signaling, AtSAUL1 and AtAGB1, were upregulated. A dehydrin (AtERD14) and a LEA protein (AtLEA26) were less abundant while two additional LEA proteins were more abundant in *PcPIP*-RNAi leaves. Three ABC transporters which are responsible for moving cutin and wax (orthologs of AtABCG11 and AtABCG15), were upregulated, providing evidence for an increase in cutinization. Four HIR/band 7 family proteins were also more abundant in *PcPIP*-RNAi leaves. These proteins are predicted to control ion channels and thereby osmotic homeostasis.

In addition to ABA, the hormonal network related to auxin and brassinosteroids appeared to be affected by PIP downregulation. Two auxin transporters, the orthologs of the *A. thaliana* auxin efflux carrier AtABCB15 and the auxin influx transporter AtAUX, were up- and downregulated, respectively. In addition, two auxin-related signaling components (AtAILP1 and AtAIR12) were more abundant. Seven proteins in the brassinosteroid network were upregulated (AtBIR1, AtBON2, AtBSK1, AtBSK2 and AtSOBIR1), and three were downregulated (AtDWF1 and AtTHE1).

The re-organization of cellular structures, including biosynthesis of the cell wall, cytoskeletal dynamics and membrane trafficking appeared to be another consequence of the reduction of PIPs. Seven enzymes involved in the biosynthesis of cell wall components were differentially regulated in the *PcPIP*-RNAi lines, with an increased and decreased abundance of the enzymes AtCALS1, AtCSLG3, AtSGT and AtSVL1 and the enzymes AtGH9A1, AtUGP2, AtUXS6, respectively. A myosin, an actin and the AtCAP1 protein, which is involved in actin dynamics, were also less abundant. The orthologs of *A. thaliana* AtSYP71, AtSYP121, AtNSF and Arf-type and Rab-type small GTPases, which are involved in intra- and inter-cellular membrane and vesicle trafficking, were upregulated.

Several differentially regulated proteins were involved in different photosynthetic processes. Of note, all of these proteins were downregulated due to the reduction of PIPs. These proteins included metabolic enzymes such as glycolytic AtTPI and AtF2KP, the photorespiratory AtSHM1 and AtAGT, and various proteins responsible for light signaling and chloroplast movement (orthologs of *A. thaliana* AtAKR2B, AtKAC1, AtNPH3, AtPMI1 and AtWEB1). Light harvesting in photosynthesis appeared to be affected because of the regulation of the AtCCD1, AtEMB1047 and AtEMB2083 proteins, which are associated with processes in photosystem II.

The downregulation of PIPs also seemed to result in an increase in the unfolded protein response (UPR), which is a cellular stress response that is related to the endoplasmic reticulum. Nine proteins that are involved in this particular stress response and are therefore responsible for proper protein folding were more abundant in the mutants: orthologs of *A. thaliana* AtBAG7, AtBIP2, AtBIP2, AtCNX1, AtERDJ3B, AtHAP6, AtPDIL1-2 and two subunits of the oligosaccharyltransferase (OST), AtSTT3A and AtSTT3B. Similarly, four ribosomal proteins were downregulated and two were less abundant.

3.3. PIP downregulation caused morphological and physiological changes in the leaf

As shown in Figure 4A, the downregulation of PIP translation caused a gradual change in leaf morphology. Compared with WT/EV, the leaves of the PIPI-9 and PIPII-13 plants were more round and less jagged, and the plants had a smaller total leaf area (Figure 4A and B); PIPII-13 plants also had a significantly smaller specific leaf area (Figure 4C). Further analysis using confocal microscopy revealed that PIPI-9 and PIPII-13 had a stomata density that was similar to WT/EV. However, the pore area, length

(L) and width (W) of the stomata in PIPI-9 (L 11.5 µm; W 2.3 µm) and PIPII-13 (L 11.1 µm; W 1.6 µm) leaves were significantly larger when compared to the stomata in WT leaves (L 10.3 µm; W 1.1 µm) and EV (L 10.3 µm; W 1.2 µm) (Figure 4E and F). This finding correlated with the wider opened stomata, as reflected by the pore size of the stomata in both lines (Figure 4D and Supplemental Figure S5).

An important physiological trait is leaf hydraulic conductance (K_{leaf}), which characterizes water permeability throughout the whole tissue and represents a central element in the regulation of the leaf water balance. We analyzed the leaf hydraulic conductance using a high pressure flow meter (HPFM). In PIPI-9 leaves, the K_{leaf} was approximately 60% higher ($P < 0.05$) compared with WT/EV leaves. The leaves of the PIPII-13 lines also tended to display a higher K_{leaf} compared with WT and EV (Supplemental Figure S4).

To analyze the importance of PIPs in plant photosynthetic processes, we analyzed the photosynthetic gas exchange under different air humidity levels (with different vapor pressure deficits (VPD) ranging from 0.75 kPa to 3.0 kPa) and under different internal leaf CO_2 concentrations ("A/Ci curves", with Ci ranging from 20 ppm to 2000 ppm). Following exposure to increasing VPD (more dry air), the leaves of the PIPI-9 lines displayed significantly ($P < 0.5$) higher transpiration rates and, accordingly, higher stomatal conductivities compared with WT/EV. The differences in transpiration and stomatal conduction increased stepwise with the rising dryness of the surrounding air (VPD from 1.4 kPa to 3.0 kPa). This physiological phenotype was not observed for line PIPII-13 (Figure 5 A and B). An analysis of the responses of photosynthesis to CO_2 revealed a significantly ($P < 0.05$) higher net CO_2 assimilation and electron transport rates in PIPI-9 and PIPII-13 compared with WT/EV when the Ci concentration ranged from ambient to high (380 ppm to 2000 ppm) (Figure 5 C and D).

The computation tools provided by Sharkey *et al.* [48] permitted the calculation of important parameters of photosynthesis and leaf physiology based on the measured A/Ci curves: V_{cmax} (the maximum carboxylation rate allowed by ribulose 1·5-bisphosphate, carboxylase/oxygenase (Rubisco)), J (the rate of photosynthetic, electron transport (based on the NADPH requirements)), TPU (triose phosphate utilization), R_d (day respiration) and g_m (mesophyll conductance to CO_2). Table 1 summarizes the values obtained by fitting the A/Ci curves of the WT/EV and *PcPIP*-RNAi lines. In comparison with WT/EV, the

photosynthetic parameters TPU, J and g_m were significantly higher in the leaves of the PIPI-9 line but not in line PIPII-13.

4. Discussion

4.1. Downregulation by RNA interference results in transcriptional and translation suppression in both PIP groups

The initial aim of this study was to reduce the two PIP groups separately by using two RNAi constructs (*PcPIP*-I-RNAi and *PcPIP*-II-RNAi). The multiple sequence alignment of the 15 *PcPIPs* and the two RNAi sequences revealed only *PIP1* genes as targets of the *PcPIP*-I-RNAi construct and only *PIP2* genes for the *PcPIP*-II-RNAi construct. However, both constructs resulted in a joint downregulation of both subgroups of PIPs. One possible explanation for this phenomenon could be that PIP1 and PIP2 function as heterotetramers and that this interaction is necessary for proper plasma membrane trafficking [52–54]. It is possible that the interaction between the PIP1 and PIP2 proteins is regulated at the expression level, and in turn, the repression of one group (PIP1 or PIP2) results in the co-suppression of the other group. Also Sade and co-workers observed reduced levels of PIP2 genes and proteins when targeting PIP1s by artificial microRNAs [8] supporting the unavoidable occurrence of co-suppression effects when targeting one PIP subgroup. In contrast to this finding, Secchi and Zwieniecki [20] demonstrated that the downregulation of PIP1 subgroup by RNAi did not result in a co-suppression of PIP2s at the transcriptional level. Therefore we cannot exclude, that the selected RNAi sequences were not sufficiently specific to target the subgroups separately, although alignment results show the intended specificity. The alignment includes only one allele of each *PIP* gene and therefore the analysis might have overlooked allelic differences and thus possible targets. In addition to the alignment, an on/off-target analysis was performed using the two RNAi sequences for a BLAST of the *P. trichocarpa* genome (Supplemental Table S2). This analysis revealed only *PIP* genes as likely targets of the 2 RNAi sequences, when assuming 100% identity for at least 21 nucleotides (Table S2). Although this analysis is quite solid, it does not ensure 100% safety because *P. trichocarpa* was used as reference. However, our RNAi approach jointly targeted the two PIP subgroups and resulted in a stable downregulation of the PIP family, supported by the almost identical pattern of PIP downregulation in the two lines PIPI-9 and PIPII-13. This

offers the novel opportunity to study the functionality of the entire PIP subfamily as also contemplated by Sade and co-workers [8].

4.2. Evidence for a central role of PIPs in stomatal movement

In the present study, we observed an excessive opening of the stomata in *PcPIP*-RNAi poplars. A few studies have described a specialized function of PIPs in regulating water flux into the guard cells of the stomata, thereby controlling opening and closure [55–57]. The stomatal movement is driven by ion fluxes, which result in an influx/efflux of water into/out of guard cells (reviewed in Kollist *et al.* [51]). PIPs ensure a high level of membrane water permeability, which is necessary for the rapid changes in guard cell volume. In addition to providing high water membrane permeability in guard cells, PIP1s, together with the activity of carbonic anhydrase and/or PEP carboxylase, may be involved in the perception of the internal CO_2 concentration [51]. The response to the internal CO_2 concentration is of central importance for stomatal control because it feeds back to photosynthetic CO_2 fixation. Thus, we speculate that the downregulation of PIP1s, besides affecting water permeability, also disrupted the perception of CO_2 in the guard cells in *PcPIP*-RNAi leaves. Consequently, the regulation of stomatal movement was affected in *PcPIP*-RNAi leaves as demonstrated with the proteomics results. An essential component of stomatal signaling mechanisms is the ABA-stimulated complex formation between the PYR/PYL/RCAR receptors (RABA) and PP2C phosphatases. This complex formation leads to the suppression of PP2C activity and, subsequently, to the activation of different kinases (OST1, CPKs and GHR1), which in turn activate the suite of anion channels [51]. Our analyses revealed several guard cell-specific signaling components (most importantly, the orthologs of *A. thaliana* AtCPK3 and AtCPK6) that were differentially regulated in *PcPIP*-RNAi leaves. However, the signaling components were not the only altered features. Several proton, anion and two sugar transporters, which also can contribute to an accumulation of solutes [58], showed a differential abundance. Although these transporters do not all have a guard cell-specific annotation, this suite of transport events strongly suggests a contribution to guard cell ion fluxes and turgor control. In summary, we hypothesize that the comprehensive reduction of PIPs disturbed the regulation of guard cell turgor. Subsequently, the reduced water membrane permeability was countered by the alteration in guard cell solute transport, which was under the control of the guard cell signaling

network. Unfortunately, this counter-regulation resulted in overcompensation and excessive stomatal opening.

4.3. Molecular implications of the disturbance in stomatal control

The dysregulation of stomatal movement as a consequence of PIP repression is followed by a set of physiological implications that begin with excessive stomatal opening (Fig. 6). Due to the wider stomatal opening, *PcPIP*-RNAi leaves exhibited higher net CO_2 assimilation and transpiration rates. The increased transpiration rates did not seem to be in balance with the water relationships in the whole plant. With the proteomic and physiological survey, we obtained evidence that the increased water loss due to transpiration caused a certain level of dehydration in the leaf, which resulted in different stress responses to increase the internal water conductivity and to decrease water loss in the leaf. First, we found several ABA biosynthesis and signaling-related proteins (AtAGB1, AtSAUL1, AtPERK4) that were differentially abundant in *PcPIP*-RNAi leaves. ABA is the most important player and starting point in guard cell signaling pathways [59], and it also regulates the water status of the plant via other pathways and controls various abiotic stress responses [60,61]. Therefore, the alteration of the ABA signalosome supports the conclusion that *PcPIP*-RNAi plants were at risk of excess water loss and drought stress. In line with this, a protein that confers drought resistance (AtABCG22) and the cutin-transporting ABC transporters (AtABCG11 and AtABCG15) were upregulated. The upregulation of cutin transporters implicates that the cuticle of *PcPIP*-RNAi leaves was reinforced, which is important for protection against drought stress [62].

In addition to the increased cutinization, the cell wall in *PcPIP*-RNAi leaves appeared to undergo remodeling because several enzymes involved in the biosynthesis of cell wall components showed a differential abundance. Interestingly, the cellulose and callose synthases, as well as the AtSVL1 protein, which is responsible for cellulose accumulation, were upregulated. This observation suggests a reinforcement of the cell wall. Additionally, the regulation of AtUGP2, AtUXS6 and AtGH9A1, enzymes that are responsible for cell wall carbohydrate biosynthesis [63–65], suggests changes in the chemical properties and composition of the cell wall. The reinforcement and restructuring of leaf cell walls is an

important dynamic response of plants to drought because adaptation of the cell wall elasticity is necessary to maintain cell turgor and extensibility [66,67].

In addition to the extracellular changes, several components of the intracellular organization were differentially regulated, including alterations in membrane trafficking and the cytoskeleton. Dynamic cytoskeleton remodeling is essential for almost every intracellular activity, from cell division to cell movement, morphogenesis and signal transduction, as well as for the transport of molecules and organelles [68,69]. Furthermore, the refinement of vesicle trafficking is needed in response to abiotic and biotic stresses, such as osmotic stress [70]. Therefore, the re-organization of cellular structures and membrane traffic in response to PIP downregulation and excess water loss trough transpiration can presumably be interpreted as drought stress defense reaction. However, intracellular management of vesicle transport is important for the localization and distribution of PIPs to/in the plasma membrane to quickly change water membrane permeability [71,72]. Most interestingly, AtSYP121, a member of the Q-SNAREs (soluble N-ethylmaleimide-sensitive factor (NSF) protein attachment protein (SNAP) receptor) and known to coordinate PIP trafficking to the plasma membrane [71], and the AtNSF protein were more abundant in *PcPIP*-RNAi leaves. This finding could reflect an attempt to compensate for the reduced PIP content by increasing intracellular vesicle transport.

Several proteins related to the unfolded protein response (UPR), which is a part of the endoplasmic reticulum (ER) quality control, were more abundant in *PcPIP*-RNAi leaves. Membrane traffic is closely associated with the ER, which is the entry point into the entire endomembrane system [73]. The UPR regulates gene transcription and protein translation to adapt the secretory pathway to ER loading and to the overall efficiency of the folding process within this compartment. Simplistically, an increase in UPR proteins can be interpreted as an accumulation of defective proteins and stress. However, other processes, such as cellular development, need for an increase in ER dimensions and, can promote similar responses [74]. However, the present study was based on plasma membrane preparations and proteomics. For data interpretation, only the plasma membrane annotated proteins were included. Therefore, the observations on UPR proteins and membrane trafficking were incomplete, and thus, important components might have been overlooked. A detailed interpretation of the other endomembrane-associated processes requires further analyses.

In addition to the extra- and intracellular re-arrangements to increase water conductivity, as well as light signaling and chloroplast movement, two important features for plants to optimize their photosynthetic capacity appeared to be affected by the reduction of PIPs: two NPH3 (non-phototropic hypocotyl 3) family proteins were downregulated in *PcPIP*-RNAi leaves. Both proteins have been shown to be involved in leaf positioning [75], auxin-dependent phototropism [76] and leaf flattening [77]. The phototropin-dependent blue light signaling pathway is also involved in controlling stomatal opening [51]. Thus, downregulation of the two NPH proteins could reflect the suppression of blue light-induced stomatal opening. In addition, three proteins (orthologs of AtWEB1 and AtPMI1) involved in chloroplast relocation [78,79] were downregulated, suggesting a reduced requirement in *PcPIP*-RNAi leaves and chloroplasts to adjust to the changing light conditions. In addition, two enzymes in the photorespiratory pathway (orthologs of the *A.thaliana* AtAGT, AtSHM1) were less abundant in *PcPIP*-RNAi leaves. Altogether, the reduced dissipation of excess photochemical energy by photorespiration and photosynthesis appeared to be better balanced in *PcPIP*-RNAi leaves, which was also supported by the observed higher rates of electron transport.

4.4. Physiological and morphological implications of the disturbance in stomatal control

The plasma membrane proteomic results suggested the presence of different strategies of the molecular machinery in response to the downregulation of PIPs which imply that leaves of *PcPIP*-RNAi plants were at risk of drought stress. These molecular observations were partially confirmed by the physiological characterization of the *PcPIP*-RNAi leaves. First, *PcPIP*-RNAi leaves displayed higher leaf hydraulic conductivity (K_{leaf}). The K_{leaf} strongly depends on several aspects of leaf anatomy, including the vein architecture, intercellular space, volume of the mesophyll and epidermis layers, and cell wall thickness and composition [80]. As suggested by the proteomic results, the cell wall and cuticle were reinforced, which not only compensates for turgor loss and prevents water loss. The cell wall modifications certainly also affected the K_{leaf}. Thus, because the K_{leaf} was higher in *PcPIP*-RNAi leaves, the cell wall modifications could be interpreted as a tactic to compensate for the reduced PIPs, which normally contribute to the internal water conductivity of the leaf. Second, in addition to the higher K_{leaf}, the mesophyll conductance for CO_2 (g_m) was also increased in *PcPIP*-RNAi leaves. This results appear to be in contrast to previous studies showing that PIP1s can facilitate CO_2 diffusion through cellular membranes

and are involved in the highly dynamic changes in g_m [17,19,20,81,82]. However, in these studies with either tobacco, Arabidopsis or Grey poplar plants, no morphological phenotype was observed. In the present study, when the PIP1 and PIP2 proteins were knocked down, the conflicting results regarding net CO_2 assimilation and g_m can be explained by the extra- and intracellular re-arrangements. The g_m reflects the integration of at least three components: conductance (i) through intercellular air spaces (g_{ias}), (ii) through the cell wall (g_w) and (iii) through the liquid phase inside cells (g_{liq}) (Flexas *et al.*, 2008, 2012). It appears evident that g_w is influenced by the cell wall structure and composition, which presumably was altered in *PcPIP*-RNAi leaves. Although there is strong support for the intracellular re-organization of the cytoskeleton in *PcPIP*-RNAi leaves, a metabolic process (e.g., carbonic anhydrase activity [83,84] most likely contributes to the potential changes in g_{liq}. However, additional details, such as cell wall thickness and composition, and the mesophyll architecture, must be assessed in future to clarify the relationship among K_{leaf}, g_m and the proteomic results.

In the present study, the leaf morphology of the lines PIPI-9 and PIPII-13 changed evidently, even when the plants were grown under normal conditions. These changes support the plasma membrane proteomic results which suggest a chronically drought-stressed phenotype due to the downregulation of PIPs. Several studies have shown that drought and ABA application reduce leaf size and SLA [85–87], as observed for *PcPIP*-RNAi leaves. However, the reduced leaf size and different shape could also be directly explained by PIP repression because PIPs are associated with cell biogenesis and growth. For instance, in barley, HvPIP1;6 facilitates growth-related water uptake into leaf epidermis elongation zone cells [88]. Furthermore, in *Arabidopsis*, AtPIP2;1 is involved in lateral root emergence [7]. However, some previous studies have shown that the modification of one specific AQP gene [9,19,81] or the repression of the PIP1 subfamily [20] does not lead to a strong visible phenotype. Therefore, we believe it is more likely that the physiological implications of PIP-downregulation caused the drought stress-adapted leaf morphology.

5. Conclusions

Globally, we could show that the reduction of PIP proteins in poplar causes multi-scale effects from the molecular to the physiological and morphological level. The dysregulation of stomatal control appeared to be the pivotal cause for the whole phenotype (Figure 6). A subsequent counter-regulation by other channels and transporters as well as signaling components led to excess stomatal opening and higher transpiration and net CO_2 assimilation rates. With the proteomic and physiological survey, we obtained evidence that the increased transpiration and water loss provoked a certain level of dehydration in the leaf. Hereupon, the hormonal network of ABA, auxin and brassinosteroids appeared to control the re-organization of extra- and intracellular structures which leaded to adjusted photosynthesis, higher K_{leaf} and an overall drought stress-adapted leaf phenotype.

Acknowledgements

We are grateful to R. Hedrich (Institute for Plant Physiology and Biophysics, University Würzburg) and F. Gaupels (BIOP, Helmholtz Centre Munich) for assistance with the data interpretation and critical discussions of the manuscript. We also thank V. Velikova (Institute of Plant Physiology and Genetics, Bulgarian Academy of Sciences) and J.B. Winkler (EUS, Helmholtz Zentrum München) for excellent technical support for the plant gas exchange measurements, and M. Spannagl and K.F.X. Mayer (PGSB, Helmholtz Zentrum München) for the on/off-target analyses of the two RNAi sequences.

This study was supported financially by the German Federal Ministry of Education and Research as part of project PRO-BIOPA (BMBF-Förderrichtlinie, Bioenergie 2021). Z.B. thanks the CSC (China Scholarship Council) Joint PhD scholarship program.

References

[1] Chaumont F, Moshelion M, Daniels MJ. Regulation of plant aquaporin activity. Biol Cell 2005;97:749–64.

[2] Heinen RB, Ye Q, Chaumont F. Role of aquaporins in leaf physiology. J Exp Bot 2009;60:2971–85.

[3] Johanson U, Karlsson M, Johansson I, Gustavsson S, Sjövall S, Fraysse L, et al. The complete set of genes encoding major intrinsic proteins in Arabidopsis provides a framework for a new nomenclature for major intrinsic proteins in plants. Plant Physiol 2001;126:1358–69.

[4] Kaldenhoff R, Ribas-Carbo M, Sans JF, Lovisolo C, Heckwolf M, Uehlein N. Aquaporins and plant water balance. Plant Cell Environ 2008;31:658–66.

[5] Maurel C, Verdoucq L, Luu D-T, Santoni V. Plant aquaporins: membrane channels with multiple integrated functions. Annu Rev Plant Biol 2008;59:595–624.

[6] Heinen RB, Bienert GP, Cohen D, Chevalier AS, Uehlein N, Hachez C, et al. Expression and characterization of plasma membrane aquaporins in stomatal complexes of Zea mays. Plant Mol Biol 2014;86:335–50.

[7] Péret B, Li G, Zhao J, Band LR, Voß U, Postaire O, et al. Auxin regulates aquaporin function to facilitate lateral root emergence. Nat Cell Biol 2012;14:991–8.

[8] Sade N, Shatil-Cohen A, Attia Z, Maurel C, Boursiac Y, Kelly G, et al. The role of plasma membrane aquaporins in regulating the bundle sheath-mesophyll continuum and leaf hydraulics. Plant Physiol 2014;166:1609–20.

[9] Perrone I, Gambino G, Chitarra W, Vitali M, Pagliarani C, Riccomagno N, et al. The grapevine root-specific aquaporin VvPIP2;4N controls root hydraulic conductance and leaf gas exchange under well-watered conditions but not under water stress. Plant Physiol 2012;160:965–77.

[10] Vandeleur RK, Mayo G, Shelden MC, Gilliham M, Kaiser BN, Tyerman SD. The role of plasma membrane intrinsic protein aquaporins in water transport through roots: diurnal and drought stress responses reveal different strategies between isohydric and anisohydric cultivars of grapevine. Plant Physiol 2009;149:445–60.

[11] Baaziz K Ben, Lopez D, Rabot A, Combes D, Gousset A, Bouzid S, et al. Light-mediated K(leaf) induction and contribution of both the PIP1s and PIP2s aquaporins in five tree species: walnut (Juglans regia) case study. Tree Physiol 2012;32:423–34.

[12] Sakr S, Alves G, Morillon R. Plasma membrane aquaporins are involved in winter embolism recovery in walnut tree. Plant Physiol 2003;133:630–41.

[13] Secchi F, Zwieniecki MA. Down-regulation of plasma intrinsic protein1 aquaporin in poplar trees is detrimental to recovery from embolism. Plant Physiol 2014;164:1789–99.

[14] Laur J, Hacke UG. Transpirational demand affects aquaporin expression in poplar roots. J Exp Bot 2013;64:2283–93.

[15] Liu J, Equiza M a, Navarro-Rodenas A, Lee SH, Zwiazek JJ. Hydraulic adjustments in aspen (Populus tremuloides) seedlings following defoliation involve root and leaf aquaporins. Planta 2014;240:553–64.

[16] Kaldenhoff R, Fischer M. Functional aquaporin diversity in plants. Biochim Biophys Acta 2006;1758:1134–41.

[17] Uehlein N, Lovisolo C, Siefritz F, Kaldenhoff R. The tobacco aquaporin NtAQP1 is a membrane CO2 pore with physiological functions. Nature 2003;425.

[18] Hanba Y, Shibasaka M. Overexpression of the barley aquaporin HvPIP2; 1 increases internal CO2 conductance and CO2 assimilation in the leaves of transgenic rice plants. Plant Cell Physiol 2004;45:521–9.

[19] Heckwolf M, Pater D, Hanson DT, Kaldenhoff R. The Arabidopsis thaliana aquaporin AtPIP1;2 is a physiologically relevant CO2 transport facilitator. Plant J 2011;67:795–804.

[20] Secchi F, Zwieniecki M a. The physiological response of Populus tremula x alba leaves to the down-regulation of PIP1 aquaporin gene expression under no water stress. Front Plant Sci 2013;4:507.

[21] Perez-Martin A, Michelazzo C, Torres-Ruiz JM, Flexas J, Fernández JE, Sebastiani L, et al. Regulation of photosynthesis and stomatal and mesophyll conductance under water stress and recovery in olive trees: correlation with gene expression of carbonic anhydrase and aquaporins. J Exp Bot 2014;65:3143–56.

[22] Isebrands JG, Richardson J. Poplars and willows: trees for society and the environment. CABI; 2014.

[23] Gilbert D. The Book Opens on the First Tree Genome 2004:1–5.

[24] Edited by Reinhard Stettler, Toby Bradshaw, Paul Heilman TH. Biology of Populus and its Implications for Management and Conservation. NRC Research Press; 1996.

[25] Chaumont F, Barrieu F, Wojcik E. Aquaporins constitute a large and highly divergent protein family in maize. Plant Physiol 2001;126:1206–15.

[26] Gupta AB, Sankararamakrishnan R. Genome-wide analysis of major intrinsic proteins in the tree plant Populus trichocarpa: characterization of XIP subfamily of aquaporins from evolutionary perspective. BMC Plant Biol 2009;9:134.

[27] Wallace I, Roberts D. Homology modeling of representative subfamilies of Arabidopsis major intrinsic proteins. Classification based on the aromatic/arginine selectivity filter. Plant Physiol 2004;135:1059–68.

[28] Higgins D, Thompson J, Gibson T. Using CLUSTAL for multiple sequence alignments. Methods Enzymol 1996;266:383–402.

[29] Lu S, Shi R, Tsao C-C, Yi X, Li L, Chiang VL. RNA silencing in plants by the expression of siRNA duplexes. Nucleic Acids Res 2004;32:e171.

[30] Axtell M, Bartel D. Antiquity of microRNAs and their targets in land plants. Plant Cell 2005;17:1658–73.

[31] Li B, Duan H, Li J, Deng XW, Yin W, Xia X. Global identification of miRNAs and targets in Populus euphratica under salt stress. Plant Mol Biol 2013;81:525–39.

[32] Ding Q, Zeng J, He X-Q. Deep sequencing on a genome-wide scale reveals diverse stage-specific microRNAs in cambium during dormancy-release induced by chilling in poplar. BMC Plant Biol 2014;14:267.

[33] Kersey PJ, Allen JE, Christensen M, Davis P, Falin LJ, Grabmueller C, et al. Ensembl Genomes 2013: scaling up access to genome-wide data. Nucleic Acids Res 2014;42:D546–52.

[34] Kinsella RJ, Kähäri A, Haider S, Zamora J, Proctor G, Spudich G, et al. Ensembl BioMarts: a hub for data retrieval across taxonomic space. Database 2011;2011:bar030.

[35] Altschul S, Madden T. Gapped BLAST and PSI-BLAST: a new generation of protein database search programs. Nucleic Acids Res 1997;25:3389–402.

[36] Meilan, Riehard; Ma C. Poplar (Populus spp.). in: Methods in Molecular Biology 2007:143–51.

[37] Behnke K, Ehlting B, Teuber M, Bauerfeind M, Louis S, Hänsch R, et al. Transgenic, non-isoprene emitting poplars don't like it hot. Plant J 2007;51:485–99.

[38] Kjellbom P, Larsson C. Preparation and polypeptide composition of chlorophyll free plasma membranes from leaves of light grown spinach and barley. Physiol Plant 1984:501–9.

[39] Widell S, Larsson C. Separation of presumptive plasma membranes from mitochondria by partition in an aqueous polymer two- phase system. Physiol Plant 1981;88:1310–6.

[40] Lundborg T, Widell S, Larsson C. Distribution of ATPases in wheat root membranes separated by phase partition. Physiol Plant 1981:89–95.

[41] Wiśniewski JR, Zougman A, Nagaraj N, Mann M. Universal sample preparation method for proteome analysis. Nat Methods 2009;6:359–62.

[42] Merl J, Ueffing M, Hauck SM, von Toerne C. Direct comparison of MS- based label- free and SILAC quantitative proteome profiling strategies in primary retinal Müller cells. Proteomics 2012;12:1902–11.

[43] Hauck SM, Dietter J, Kramer RL, Hofmaier F, Zipplies JK, Amann B, et al. Deciphering membrane-associated molecular processes in target tissue of autoimmune uveitis by label-free quantitative mass spectrometry. Mol Cell Proteomics 2010;9:2292–305.

[44] Hahne H, Moghaddas Gholami A, Kuster B. Discovery of O-GlcNAc-modified proteins in published large-scale proteome data. Mol Cell Proteomics 2012;11:843–50.

[45] Vizcaíno JA, Deutsch EW, Wang R, Csordas A, Reisinger F, Ríos D, et al. ProteomeXchange provides globally coordinated proteomics data submission and dissemination. Nat Biotechnol 2014;32:223–6.

[46] Ethier GJ, Livingston NJ. On the need to incorporate sensitivity to CO2 transfer conductance into the Farquhar–von Caemmerer–Berry leaf photosynthesis model. Plant Cell Environ 2004;27:137–53.

[47] Ethier GJ, Livingston NJ, Harrison DL, Black TA, Moran JA. Low stomatal and internal conductance to CO2 versus Rubisco deactivation as determinants of the photosynthetic decline of ageing evergreen leaves. Plant Cell Environ 2006;29:2168–84.

[48] Sharkey TD, Bernacchi CJ, Farquhar GD, Singsaas EL. Fitting photosynthetic carbon dioxide response curves for C3 leaves. Plant Cell Environ 2007;30:1035–40.

[49] Tsuda M, Tyree MT. Plant hydraulic conductance measured by the high pressure flow meter in crop plants. J Exp Bot 2000;51:823–8.

[50] Kiernan JA. Formaldehyde, formalin, paraformaldehyde and glutaraldehyde: what they are and what they do. Micros Today 2000;1.

[51] Kollist H, Nuhkat M, Roelfsema MRG. Closing gaps: linking elements that control stomatal movement. New Phytol 2014;203:44–62.

[52] Fetter K, Wilder V Van. Interactions between plasma membrane aquaporins modulate their water channel activity. Plant Cell 2004;16:215–28.

[53] Zelazny E, Borst JW, Muylaert M, Batoko H, Hemminga MA, Chaumont F. FRET imaging in living maize cells reveals that plasma membrane aquaporins interact to regulate their subcellular localization. Proc Natl Acad Sci 2007;104:12359–64.

[54] Horie T, Kaneko T, Sugimoto G, Sasano S, Panda SK, Shibasaka M, et al. Mechanisms of water transport mediated by PIP aquaporins and their regulation via phosphorylation events under salinity stress in barley roots. Plant Cell Physiol 2011;52:663–75.

[55] Kaldenhoff R, Kölling A, Meyers J, Karmann U, Ruppel G, Richter G. The blue light-responsive AthH2 gene of Arabidopsis thaliana is primarily expressed in expanding as well as in differentiating cells and encodes a putative channel protein of the plasmalemma. Plant J 1995;7:87–95.

[56] Fraysse LC, Wells B, McCann MC, Kjellbom P. Specific plasma membrane aquaporins of the PIP1 subfamily are expressed in sieve elements and guard cells. Biol Cell 2005;97:519–34.

[57] Sun M, Xu W, Zhu Y, Su W, Tang Z. A simple method forIn Situ hybridization to RNA in guard cells of Vicia Faba L.: The expression of aquaporins in guard cells. Plant Mol Biol Report 2001:129–35.

[58] Pandey S, Zhang W, Assmann SM. Roles of ion channels and transporters in guard cell signal transduction. FEBS Lett 2007;581:2325–36.

[59] Kim T-H, Maik BĆ. Guard cell signal transduction network: advances in understanding abscisic acid, CO2, and Ca2+ signaling. Annu Rev Plant Biol 2010;61:561.

[60] Tuteja N. Abscisic acid and abiotic stress signaling. Plant Signal Behav 2007;2:135–8.

[61] Zhang JZ, Creelman RA, Zhu J-K. from laboratory to field. Using Information from Arabidopsis to Engineer Salt, Cold, and Drought Tolerance in Crops. Plant Physiol 2004;135:615–21.

[62] Yeats TH, Rose JKC. The formation and function of plant cuticles. Plant Physiol 2013;163:5–20.

[63] Park J-I, Ishimizu T, Suwabe K, Sudo K, Masuko H, Hakozaki H, et al. UDP-glucose pyrophosphorylase is rate limiting in vegetative and reproductive phases in Arabidopsis thaliana. Plant Cell Physiol 2010;51:981–96.

[64] Oikawa A, Joshi HJ, Rennie EA, Ebert B, Manisseri C, Heazlewood JL, et al. An integrative approach to the identification of Arabidopsis and rice genes involved in xylan and secondary wall development. PLoS One 2010;5:e15481.

[65] Mansoori N, Timmers J, Desprez T. KORRIGAN1 Interacts Specifically with Integral Components of the Cellulose Synthase Machinery. PLoS One 2014;9:e112387.

[66] Moore JP, Vicré-Gibouin M, Farrant JM, Driouich A. Adaptations of higher plant cell walls to water loss: drought vs desiccation. Physiol Plant 2008;134:237–45.

[67] Tenhaken R. Cell wall remodeling under abiotic stress. Front Plant Sci 2015;5:771.

[68] Verchot-Lubicz J, Goldstein RE. Cytoplasmic streaming enables the distribution of molecules and vesicles in large plant cells. Protoplasma 2010;240:99–107.

[69] Wang Z, Meng P, Zhang X, Ren D, Yang S. BON1 interacts with the protein kinases BIR1 and BAK1 in modulation of temperature-dependent plant growth and cell death in Arabidopsis. Plant J 2011;67:1081–93.

[70] Mazel A, Leshem Y, Tiwari B, Levine A. Induction of salt and osmotic stress tolerance by overexpression of an intracellular vesicle trafficking protein AtRab7 (AtRabG3e). Plant Physiol 2004;134:118–28.

[71] Hachez C, Laloux T, Reinhardt H, Cavez D, Degand H, Grefen C, et al. Arabidopsis SNAREs SYP61 and SYP121 coordinate the trafficking of plasma membrane aquaporin PIP2;7 to modulate the cell membrane water permeability. Plant Cell 2014;26:3132–47.

[72] Luu D, Martiniere A, Sorieul M, Runions J, Maurel C. Fluorescence recovery after photobleaching reveals high cycling dynamics of plasma membrane aquaporins in Arabidopsis roots under salt stress. Plant J 2012;69:894–905.

[73] Jürgens G. Membrane trafficking in plants. Annu Rev Cell Dev Biol 2004;20:481–504.

[74] Vitale A, Boston RS. Endoplasmic reticulum quality control and the unfolded protein response: insights from plants. Traffic 2008;9:1581–8.

[75] Inoue S, Kinoshita T, Takemiya A, Doi M, Shimazaki K. Leaf positioning of Arabidopsis in response to blue light. Mol Plant 2008;1:15–26.

[76] Wan Y, Jasik J, Wang L, Hao H, Volkmann D, Menzel D, et al. The signal transducer NPH3 integrates the phototropin1 photosensor with PIN2-based polar auxin transport in Arabidopsis root phototropism. Plant Cell 2012;24:551–65.

[77] Kozuka T, Suetsugu N, Wada M, Nagatani A. Antagonistic regulation of leaf flattening by phytochrome B and phototropin in Arabidopsis thaliana. Plant Cell Physiol 2013;54:69–79.

[78] Kodama Y, Suetsugu N, Kong S-G, Wada M. Two interacting coiled-coil proteins, WEB1 and PMI2, maintain the chloroplast photorelocation movement velocity in Arabidopsis. Proc Natl Acad Sci U S A 2010;107:19591–6.

[79] DeBlasio S, Luesse D, Hangarter R. A plant-specific protein essential for blue-light-induced chloroplast movements. Plant Physiol 2005;139:101–14.

[80] Aasamaa K, Niinemets Ü, Sõber A. Leaf hydraulic conductance in relation to anatomical and functional traits during Populus tremula leaf ontogeny. Tree Physiol 2005:1409–18.

[81] Flexas J, Ribas-Carbó M, Hanson DT, Bota J, Otto B, Cifre J, et al. Tobacco aquaporin NtAQP1 is involved in mesophyll conductance to CO2 in vivo. Plant J 2006;48:427–39.

[82] Kelly G, Sade N, Attia Z, Secchi F, Zwieniecki M, Holbrook NM, et al. Relationship between hexokinase and the aquaporin PIP1 in the regulation of photosynthesis and plant growth. PLoS One 2014;9:e87888.

[83] Flexas J, Ribas-Carbó M, Diaz-Espejo A, Galmés J, Medrano H. Mesophyll conductance to CO2: current knowledge and future prospects. Plant Cell Environ 2008;31:602–21.

[84] Flexas J, Barbour MM, Brendel O, Cabrera HM, Carriquí M, Díaz-Espejo A, et al. Corrigendum to "Mesophyll diffusion conductance to CO2: An unappreciated central player in photosynthesis." Plant Sci 2012;196:31.

[85] Marron N, Dreyer E. Impact of successive drought and re-watering cycles on growth and specific leaf area of two Populus× canadensis (Moench) clones,'Dorskamp'and "Luisa_Avanzo." Tree Physiol 2003;23:1225–35.

[86] Monclus R, Villar M. Productivity, water-use efficiency and tolerance to moderate water deficit correlate in 33 poplar genotypes from a Populus deltoides× Populus trichocarpa F1 progeny. Tree Physiol 2009;29:1329–39.

[87] Yin C, Duan B, Wang X, Li C. Morphological and physiological responses of two contrasting poplar species to drought stress and exogenous abscisic acid application. Plant Sci 2004;167:1091–7.

[88] Wei W, Alexandersson E, Golldack D, Miller AJ, Kjellbom PO, Fricke W. HvPIP1;6, a barley (Hordeum vulgare L.) plasma membrane water channel particularly expressed in growing compared with non-growing leaf tissues. Plant Cell Physiol 2007;48:1132–47.

[89] Maierhofer T, Diekmann M, Offenborn JN, Lind C, Bauer H, Hashimoto K, et al. Site-and kinase-specific phosphorylation-mediated activation of SLAC1, a guard cell anion channel stimulated by abscisic acid. Sci Signal 2014;7:ra86–ra86.

[90] Yang K, Wang H, Xue S, Qu X, Zou J, Le J. Requirement for A-type cyclin-dependent kinase and cyclins for the terminal division in the stomatal lineage of Arabidopsis. J Exp Bot 2014;65:2449–61.

[91] Jungkunz IM. Funktionelle Untersuchungen zum cytosolischen Hsp70-Hsp40-Chaperonsystem in Arabidopsis thaliana. Erlangen, Nürnberg, Univ., Diss., 2011; 2011.

[92] Uraji M, Katagiri T, Okuma E, Ye W, Hossain MA, Masuda C, et al. Cooperative function of PLDδ and PLDα1 in abscisic acid-induced stomatal closure in Arabidopsis. Plant Physiol 2012;159:450–60.

[93] Kim Y-M, Han Y-J, Hwang O-J, Lee S-S, Shin A-Y, Kim SY, et al. Overexpression of Arabidopsis translationally controlled tumor protein gene AtTCTP enhances drought tolerance with rapid ABA-induced stomatal closure. Mol Cells 2012;33:617–26.

[94] Kollist H, Nuhkat M. Tansley review Closing gaps : linking elements that control stomatal movement. New Phytol 2014.

[95] Tang H, Vasconcelos A, Berkowitz G. Physical association of KAB1 with plant K+ channel alpha subunits. Plant Cell 1996;8:1545–53.

[96] Guo F, Young J, Crawford N. The nitrate transporter AtNRT1. 1 (CHL1) functions in stomatal opening and contributes to drought susceptibility in Arabidopsis. Plant Cell Online 2003;15:107–17.

[97] Stadler R, Büttner M, Ache P. Diurnal and light-regulated expression of AtSTP1 in guard cells of Arabidopsis. Plant Physiol 2003;133:528–37.

[98] Talbott L, Zeiger E. The role of sucrose in guard cell osmoregulation. J Exp Bot 1998;49:329–37.

[99] Li Z-Y, Xu Z-S, He G-Y, Yang G-X, Chen M, Li L-C, et al. The Voltage-Dependent Anion Channel 1 (AtVDAC1) Negatively Regulates Plant Cold Responses during Germination and Seedling Development in Arabidopsis and Interacts with Calcium Sensor CBL1. Int J Mol Sci 2013;14:701–13.

[100] Allen GJ, Chu SP, Schumacher K, Shimazaki CT, Vafeados D, Kemper A, et al. Alteration of stimulus-specific guard cell calcium oscillations and stomatal closing in Arabidopsis det3 mutant. Science (80-) 2000;289:2338–42.

[101] Allen GJ, Chu SP, Harrington CL, Schumacher K, Hoffmann T, Tang YY, et al. A defined range of guard cell calcium oscillation parameters encodes stomatal movements. Nature 2001;411:1053–7.

[102] Pei Z, Ward J, Schroeder J. Magnesium sensitizes slow vacuolar channels to physiological cytosolic calcium and inhibits fast vacuolar channels in fava bean guard cell vacuoles. Plant Physiol 1999;121:977–86.

[103] Qin P, Tu B, Wang Y, Deng L, Quilichini TD, Li T, et al. ABCG15 encodes an ABC transporter protein, and is essential for post-meiotic anther and pollen exine development in rice. Plant Cell Physiol 2013;54:138–54.

[104] Duan Y, Guo J, Shi X, Guan X, Liu F, Bai P, et al. Wheat hypersensitive-induced reaction genes TaHIR1 and TaHIR3 are involved in response to stripe rust fungus infection and abiotic stresses. Plant Cell Rep 2013;32:273–83.

[105] Liepman AH, Olsen LJ. Peroxisomal alanine : glyoxylate aminotransferase (AGT1) is a photorespiratory enzyme with multiple substrates in Arabidopsis thaliana. Plant J 2001;25:487–98.

[106] Valente MAS, Faria J a Q a, Soares-Ramos JRL, Reis P a B, Pinheiro GL, Piovesan ND, et al. The ER luminal binding protein (BiP) mediates an increase in drought tolerance in soybean and delays drought-induced leaf senescence in soybean and tobacco. J Exp Bot 2009;60:533–46.

Figure legends

Figure 1. Proteomic analysis of PIP protein abundance in *PcPIP*-RNAi lines. The Log_2 ratio of PIP protein abundance in *PcPIP*-RNAi transgenic lines (TR) relative to empty vector (EV) determined by LC-MS/MS-based proteomic analysis. Eleven of 15 PIP proteins were detected. The data represent the 2 *PcPIP*-RNAi transgenic lines (PIPI-9■ and PIPII-13■) that showed lowest PIP protein abundance.

Figure 2. Score (**A**) and loading (**B**) plots for the orthogonal partial least squares-discriminant analysis (OPLS-DA) based on plasma membrane proteins extracted from the leaves of wild type and transgenic *PcPIP*-RNAi poplars. (**A**) Each point represents an independent plant sample (n=4 in the score plots): wild type (WT ●), empty vector control (EV ●), and two *PcPIP*-RNAi-lines (PIPI-9 ▼, PIPII-13 ▲). (**B**) Each point represents one of the 510 proteins included in the analysis. Proteins marked in orange have a Variable of Importance for the Projection value (VIP value) greater than 1 and were therefore defined as discriminant proteins. The model summary provided the following: R2X(1)=0.222, R2X(cum)=0.578, R2Y(cum)=1, Q2(cum)=0.951 and CV-ANOVA; P = 0.00012.

Figure 3. Functional categorization of 167 discriminant proteins (VIP value > 1) identified by the OPLS-DA model of plasma membrane proteins extracted from wild type and transgenic *PcPIP*-RNAi poplar leaves. (**A**) The GO SLIM classification was obtained via the TAIR DB search. The results for the category “Biological Process” are shown. (**B**) Classification based on TAIR annotation and available literature information.

Figure 4. Leaf morphology of *PcPIP*-RNAi transgenic lines (PIPI-9 and PIPII-13), empty vector (EV) and wild type (WT) plants. (**A**) No. 1-8 and no. 11-15 leaf morphology. (**B**) Total leaf area. (C) Specific leaf area (SLA) of leaf no. 9. (**D**) Stomatal density. (**E**) Stomatal pore opening area. (**F**) Stomatal pore length (solid filled in) and width (grid filled in). For (**B**) and (**C**) values area mean of 6 biological replicates ± SE. For (**D**) to (**F**) 30 randomly selected stomata of 3 biological replicates were analyzed (n=3, means ± SE). (*) indicates significant difference between *PcPIP*-RNAi transgenic and wild type plants (one-way ANOVA, $P < 0.05$).

Figure 5. Photosynthetic parameters of leaf no. 9 for wild type and *PcPIP*-RNAi transgenic plants (wild type (●), empty vector (●), PIPI-9 (▼) and PIPII-13 (▲)) during water curves (different leaf-to-air vapor pressure deficit (VPD), (**A**), (**B**)) and A/Ci curves (different internal CO_2 concentration (C_i), (**C**), (**D**)). (**A**) Transpiration rate. (**B**) Stomatal conductance for H_2O. (**C**) Net CO_2 assimilation rate. (**D**) Electron transport rate (ETR). Values are the means +SE (n=6). (*) indicates significant difference between *PcPIP*-RNAi transgenic and wild type plants (one-way ANOVA, $P < 0.05$).

Figure 6. Summary of the consequences of the complete downregulation of PIP proteins in poplar leaves. Green boxes show the results of the physiological analyses, red boxes display the molecular observation based on the proteomic analyses, and grey boxes show the potential mechanisms underlying the phenotypes caused by the reduction of PIP.

Table legend

Table 1. Characterization of the photosynthetic parameters of wild type and *PcPIP*-RNAi transgenic plants by the curve-fitting method for A/Ci curves (Ethier and Livingston, 2004; Ethier et al., 2006) by applying the online tool described by Sharkey et al. (2007). V_{cmax}, maximum carboxylation rate allowed by ribulose 1·5-bisphosphate carboxylase/oxygenase (Rubisco); J, rate of photosynthetic electron transport (based on the NADPH requirements); TPU, triose phosphate use; R_d, day respiration; g_m, mesophyll conductance of CO_2. (*) indicates significant difference between the transgenic line and wild type (one-way ANOVA, $P < 0.05$). Values are the means ±SE (n=6).

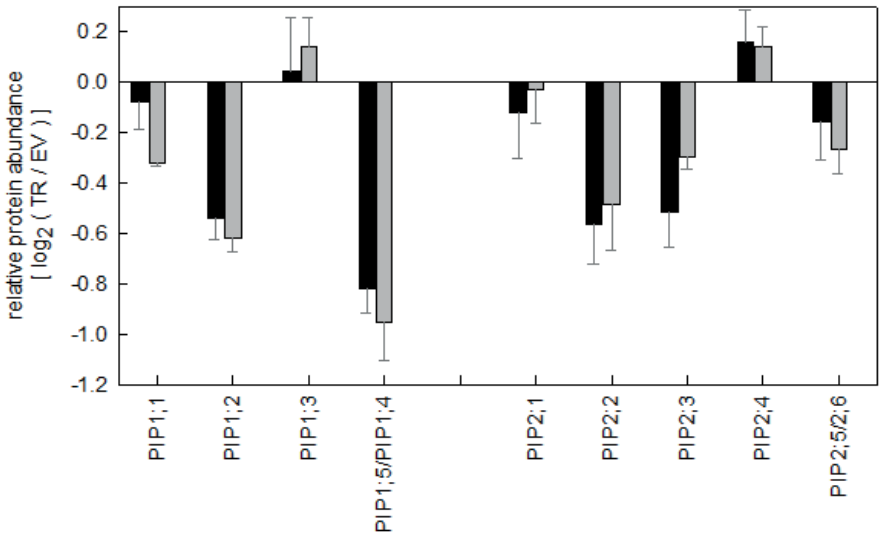

Figure 1

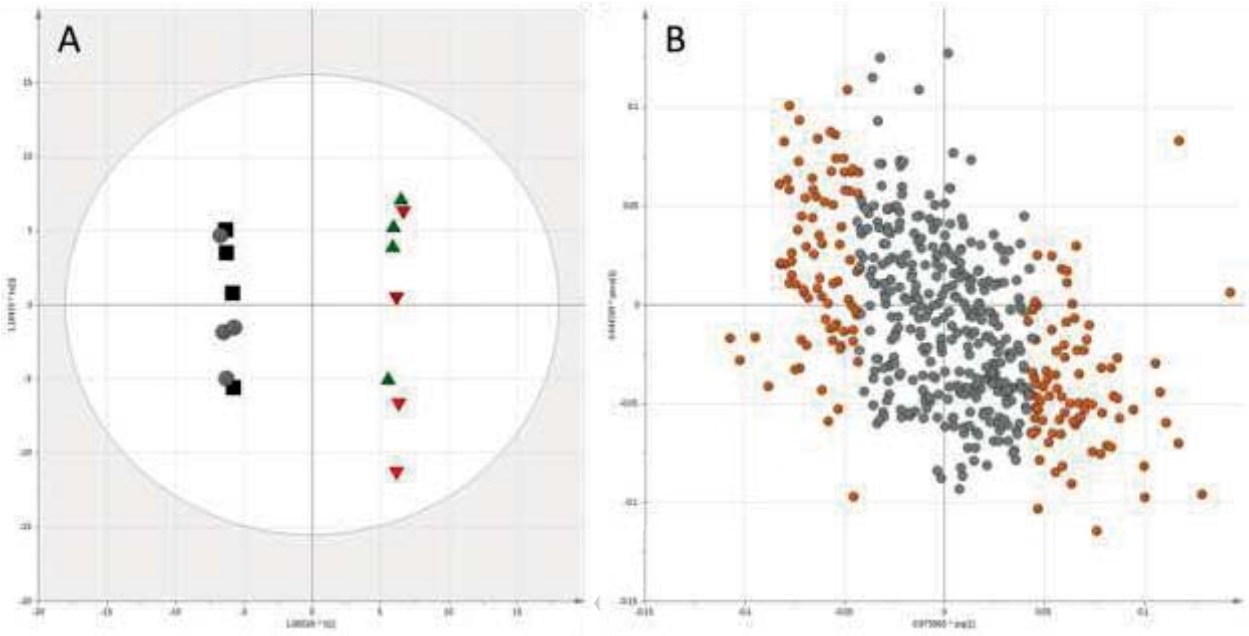

Figure 2

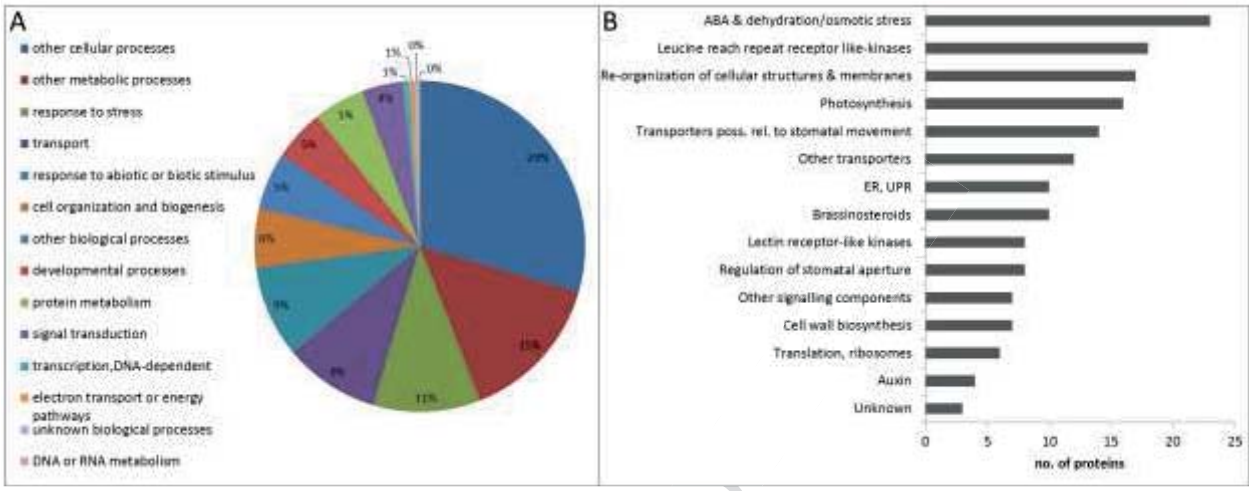

Figure 3

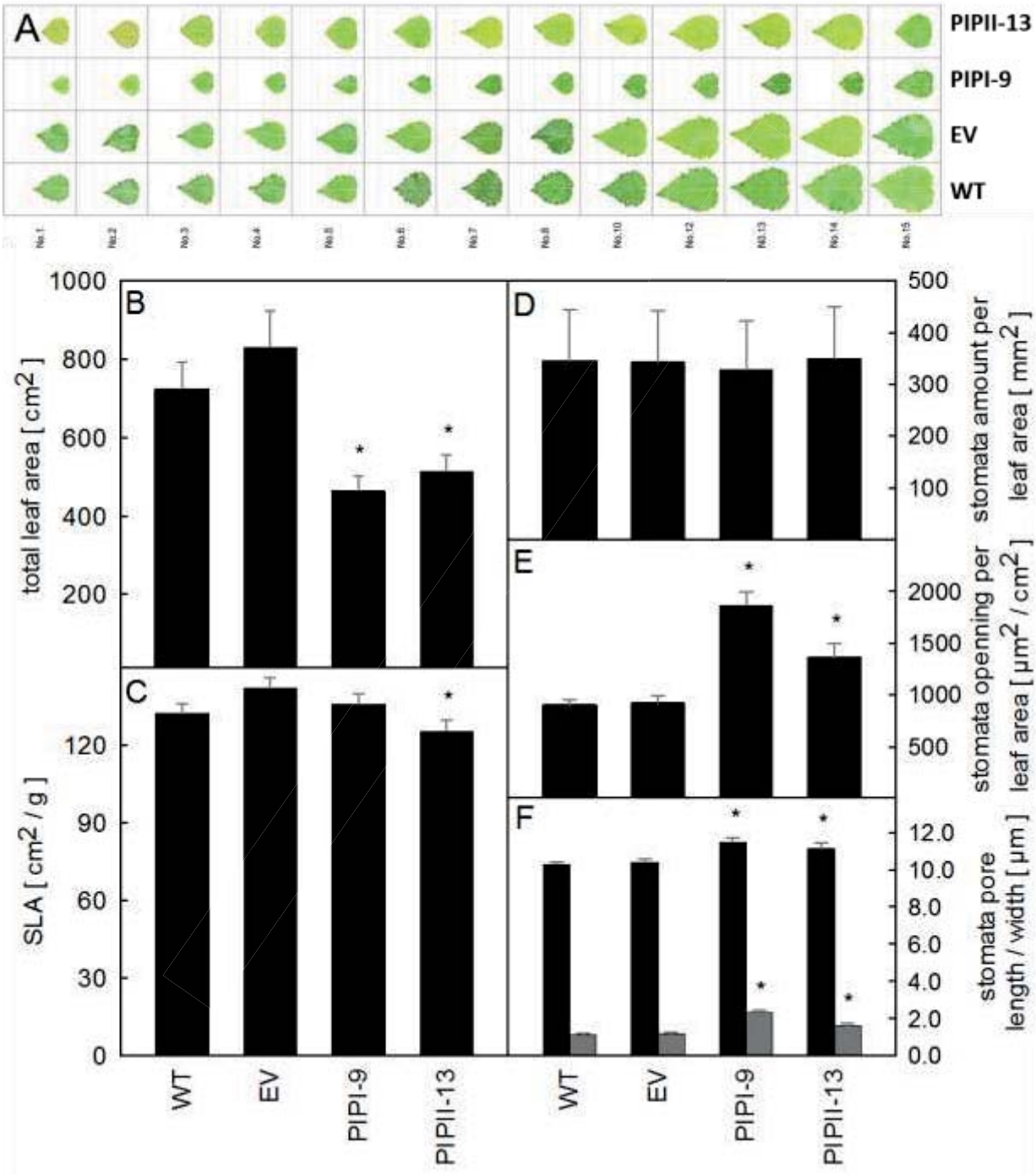

Figure 4

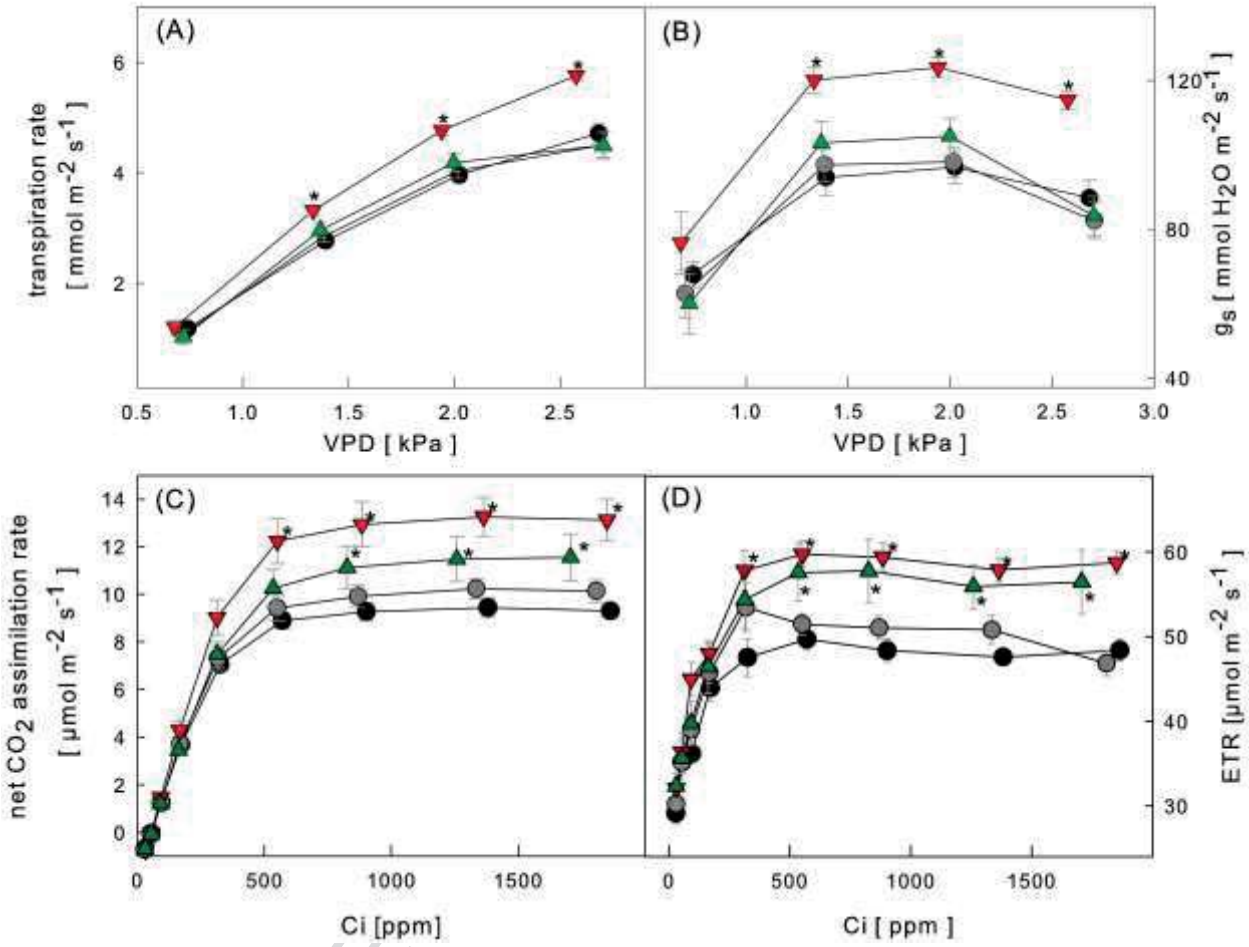

Figure 5

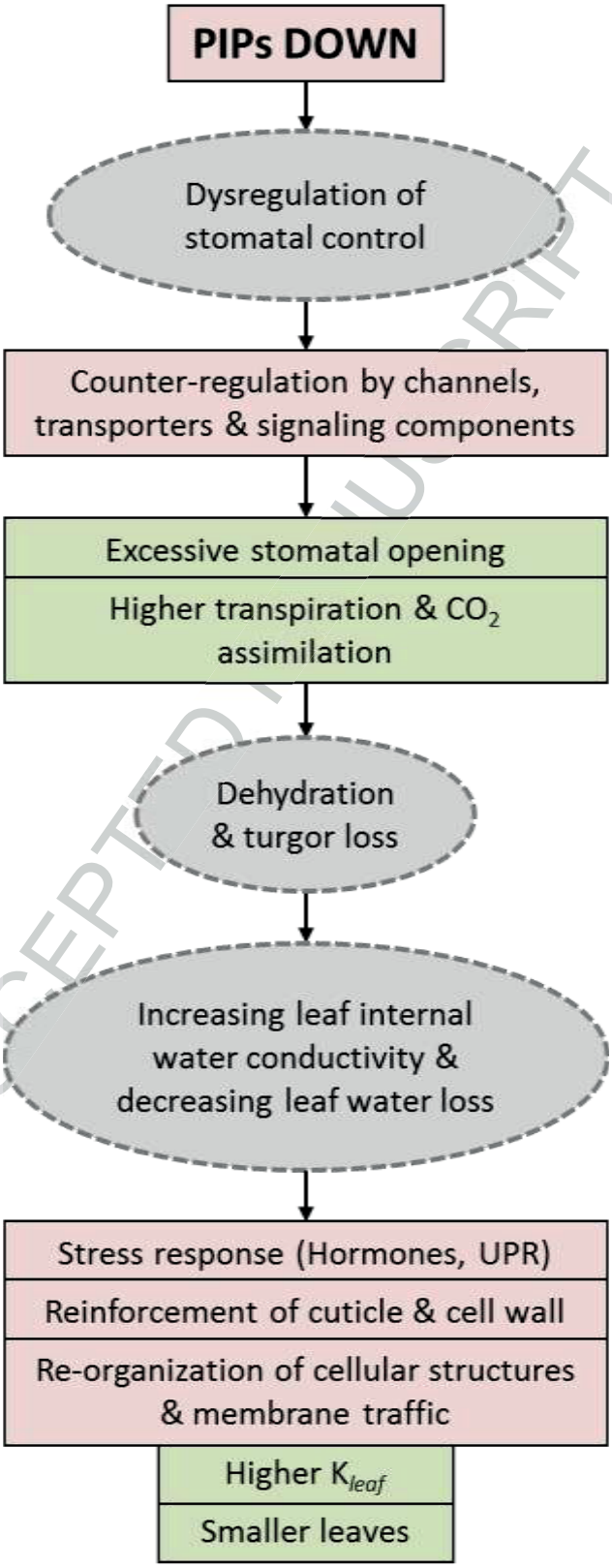

Figure 6

TABLES

Table 1

	$V_{c\,max}$ ($\mu mol\ m^{-2}\ s^{-1}$)	J ($\mu mol\ m^{-2}\ s^{-1}$)	TPU ($\mu mol\ m^{-2}\ s^{-1}$)	R_d ($\mu mol\ m^{-2}\ s^{-1}$)	g_m ($mol\ m^{-2}\ s^{-1}$)
WT	46.47±1.52	52.52±1.95	3.45±0.12	0.99±0.07	0.06±0.00
EMPTY	50.21±1.81	57.26±2.80	3.72±0.17	1.17±0.10	0.06±0.01
PIPI-9	44.09±6.49	66.87±6.03*	4.69±0.32*	0.89±0.13	0.14±0.02*
PIPII-13	50.25±3.08	61.46±3.59	4.21±0.27	1.15±0.07	0.06±0.00

Characterization of the photosynthetic parameters of wild type and *PcPIP*-RNAi transgenic plants by the curve-fitting method for A/Ci curves (Ethier and Livingston, 2004; Ethier et al., 2006) by applying the online tool described by Sharkey et al. (2007). V_{cmax}, maximum carboxylation rate allowed by ribulose 1·5-bisphosphate carboxylase/oxygenase (Rubisco); J, rate of photosynthetic electron transport (based on the NADPH requirements); TPU, triose phosphate use; R_d, day respiration; g_m, mesophyll conductance of CO_2. (*) indicates significant difference between the transgenic line and wild type (one-way ANOVA, $P < 0.05$). Values are the means ±SE (n=6).

Biological significance

The present work is a comprehensive survey combining leaf plasma membrane proteomics and physiological methods to assess the functionality of the whole PIP subfamily in tree model system.

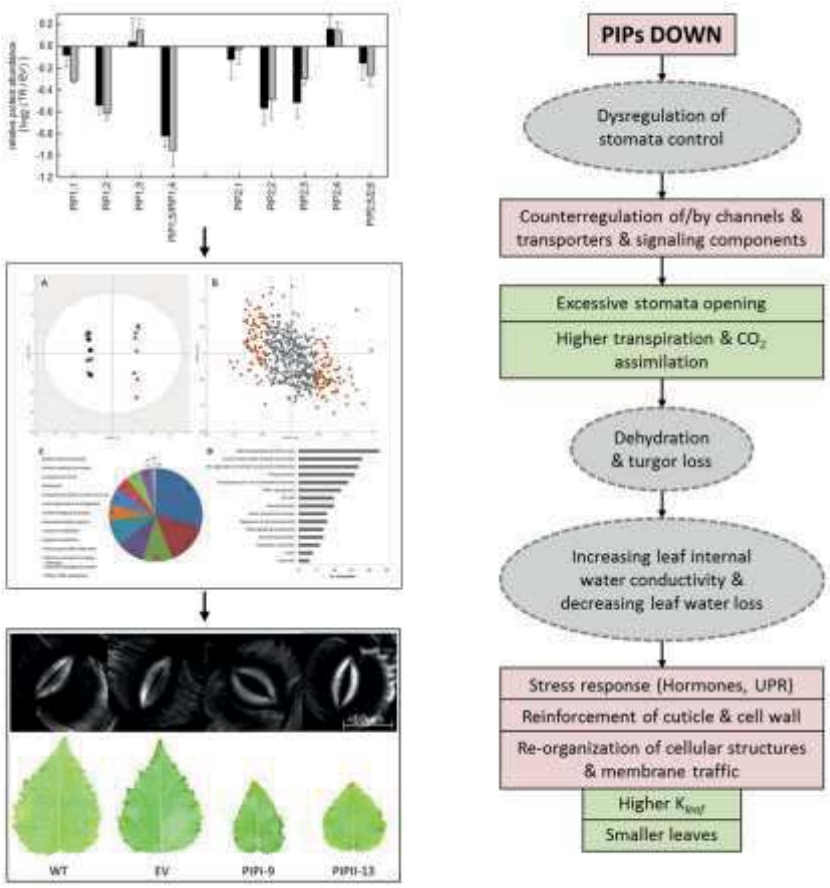

Graphical abstract

Highlights

- We established *PcPIP*-RNAi-poplars targeting the whole PIP subfamily
- PIP downregulation strongly affected the leaf plasma membrane proteome
- Signaling components and transporters involved in stomatal movement were changed
- Leaves exhibited excessive stomata opening
- As consequence, leaf physiology was affected on multi-scale